Device

Article

Operando quantum sensing captures the nanoscale electrochemical evolution in batteries

Graphical abstract

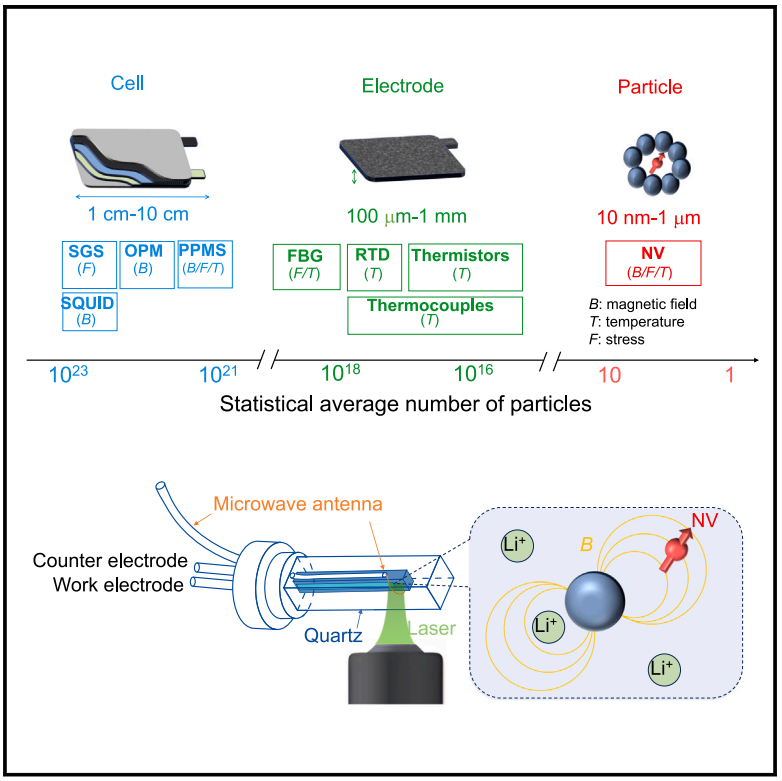

Highlights

- Propose an *in situ* diamond NV center-based quantum sensing technology for batteries
- Design an integrated battery device for *in situ* quantum sensing
- *Operando* monitor nanoscale magnetic signals in electrode duration battery operation
- Develop multi-threaded monitoring to enable high-resolution mapping in electrode

Authors

Binghang Liu, Xiu-Qi Chen, Yan-Xing Shang, Xiaolin Xiong, Huijie Zheng, Gang-Qin Liu, Liumin Suo

Correspondence

hjzheng@iphy.ac.cn (H.Z.),
gqliu@iphy.ac.cn (G.-Q.L.),
suoliumin@iphy.ac.cn (L.S.)

In brief

Operando capturing the nanoscale electrochemical evolution in the battery is challenging due to the lack of real-time and non-destructive detection methods with sufficient spatial resolution and sensitivity. Herein, we provided a methodology for *in situ* non-destructive battery characterization using diamond NV center-based quantum sensing technology to obtain information on nanoscale microregions within the electrode. Our work offers a brand-new route for high-resolution, sensitive, and multi-thread monitoring nanoscale electrochemical evolution in batteries.

Develop
Prototype with demonstrated applications in relevant environment

Liu et al., 2024, Device *2*, 100521
December 20, 2024
https://doi.org/10.1016/j.device.2024.100521

CellPress

Please cite this article in press as: Liu et al., *Operando* quantum sensing captures the nanoscale electrochemical evolution in batteries, Device (2024), https://doi.org/10.1016/j.device.2024.100521

Device

CellPress
OPEN ACCESS

Article

Operando quantum sensing captures the nanoscale electrochemical evolution in batteries

Binghang Liu,[1,2,6] Xiu-Qi Chen,[1,3,6] Yan-Xing Shang,[1] Xiaolin Xiong,[1,2] Huijie Zheng,[1,*] Gang-Qin Liu,[1,4,5,*] and Liumin Suo[1,2,7,*]

[1]Beijing National Laboratory for Condensed Matter Physics, Institute of Physics, Chinese Academy of Science, Beijing 100190, China
[2]Center of Materials Science and Optoelectronics Engineering, University of Chinese Academy of Sciences, Beijing 100049, China
[3]China School of Physical Science, University of Chinese Academy of Sciences, Beijing 100049, China
[4]CAS Center of Excellence in Topological Quantum Computation, Beijing 100190, China
[5]Songshan Lake Materials Laboratory, Dongguan, Guangdong 523808, China
[6]These authors contributed equally
[7]Lead contact
*Correspondence: hjzheng@iphy.ac.cn (H.Z.), gqliu@iphy.ac.cn (G.-Q.L.), suoliumin@iphy.ac.cn (L.S.)
https://doi.org/10.1016/j.device.2024.100521

THE BIGGER PICTURE Electrode particles are the most minor functional units of a battery. Their failure and non-uniformity significantly impact battery performance according to the barrel principle. Therefore, sensing at the particle level is crucial for accurately assessing the state of the battery. However, current sensors cannot achieve single-particle spatial resolution. Our proposed methodology, applying diamond NV center-based quantum sensing technology to the *in situ*, non-destructive characterization of batteries, has the potential to address this issue. Diamond NV centers have incredibly high resolution (~1 nm to ~1 μm) and are highly sensitive to critical physical parameters within the battery, such as temperature, stress, and magnetic fields. This technology is poised to become a multifunctional sensor inside electrodes, holding significant promise for future research into battery materials, failure mechanisms, and lifespan prediction.

SUMMARY

Obtaining the electrode particle level information is an essential prerequisite for diagnosing battery failures and assessing their state of health (SOH). However, detecting the electrochemical evolution of particles at the nanoscale is not yet possible due to the lack of real-time and non-destructive detection methods with sufficient spatial resolution and sensitivity. Here, we propose an *operando* quantum sensing approach in which diamond nitrogen-vacancy (NV) centers are embedded directly into the internal electrodes to detect the electrochemical evolution at the particle level. The proof of the concept is experimentally demonstrated on an Fe_3O_4 electrode, where the nanoscale electrochemical evolution is detected by monitoring the magnetic stray field from nearby electrode particles. Multithreading monitoring achieves a spatially resolved measurement of the internal magnetic field, revealing the heterogeneous reaction kinetics among the individual particles. Our work provides a brand-new route for high-resolution, sensitive, and multi-thread monitoring of nanoscale electrochemical evolution in batteries.

INTRODUCTION

Massive, diverse electrode particles as the minimum functional unit integrate batteries where the available electrochemical performance indicators and their relative measurable physical parameters (stress, temperature, and magnetic field) are statistical averages of the whole device, ignoring the diversity of individual active particles. According to the wooden bucket principle, such deviation is a major cause of failure to accurately diagnose, evaluate, and predict the electrochemical evolution under actual operating conditions, as the weakest particles determine battery degradation. Therefore, it is imperative to realize the microscopic observation of the electrochemical evolution at the particle level. It would provide a basis for assessing batteries' state of charge (SOC) and state of health (SOH) in practice. Unfortunately, the detection of electrochemical evolution at the level of individual

Please cite this article in press as: Liu et al., *Operando* quantum sensing captures the nanoscale electrochemical evolution in batteries, Device (2024), https://doi.org/10.1016/j.device.2024.100521

particles is still not feasible due to the lack of non-destructive real-time detection methods with sufficient spatial resolution and sensitivity.[1]

So far, almost all available sensing technologies used in battery characterization are too large to focus on the nanodomain in the electrodes,[1,2] such as strain gauge sensors[3–5] for stress measurement, thermocouples[6,7] for temperature, and physical property measurement systems (PPMSs)[8,9] for magnetic field. Even the advanced embeddable fiber Bragg grating (FBG) sensors[10–18] can miniaturize one dimension to hundreds of micrometers for internal electrode scale, and their spatial resolution is far from the requirements of nanoscale electrochemical evaluation. Meanwhile, considering that the sensor is embedded in the electrode particles' complex electrochemical, chemical, and mechanical environment, it must have high chemical inertness and physical stability against the electrolyte and not damage the microscopically embedded areas of the electrode.[19]

Based on the abovementioned, the first challenge of *operando* battery sensing is to miniaturize an electrochemically inert sensor to achieve particle-scale spatial resolution (nanometer to micrometer) and to enable the detection of *in situ* signals from nearby particles. Furthermore, the second challenge is to implant enough non-destructive detection sensors with a simple and efficient approach to realize multithreading monitoring for high-space-resolution electrode mapping because the high spatial resolution is incompatible with a large detection zone,[19] which has a detrimental effect on analyzing the correlation between the degradation of the whole battery and the individual electrode particles.

Quantum sensing with diamond nitrogen-vacancy (NV) centers can meet the above requirements.[20–25] Diamond sensors can provide a tiny sensing volume (nanometer to micrometer), enabling an extremely high spatial resolution. The optical interface allows widespread use within electrodes, enabling multi-threaded detection. The diamond material itself is robust, chemically stable, and can be used in almost all environments, ensuring its reliability.[26,27] The spin state of an NV center is sensitive to local physical parameters, including magnetic fields,[28–31] temperature,[32–35] pressure,[36–38] and electric fields.[39,40] This opens up promising perspectives for NV-based battery characterization. NV centers have been proposed as an *in situ* ion concentration sensor[41] and as a sensor for static electric fields in the electrolyte.[42] However, addressing the compatibility issues between the diamond NV center-based quantum sensing system and battery system is challenging, such as introducing a microwave antenna and laser inside the battery.

In this work, we developed an integrated NV-battery detection device and performed *in situ* magnetic field measurements during battery discharge. The spatially resolved electrochemical reaction process (Fe_3O_4 → FeO → Fe) of an Fe_3O_4 electrode was successfully tracked with NV-based quantum sensors, providing rich, detailed information compared to the results of macroscopic electrochemical measurements. The feasibility of high-resolution, non-destructive *in situ* microregions and large-area detection through multithreading monitoring within the battery electrodes was demonstrated.

RESULTS

Nanoscale quantum sensor for the battery

As summarized in Figure 1A, battery scale (1 cm to about 10 cm) and electrode scale (100 μm to 1 mm) sensors have been well developed and used. However, their signal is a statistical average of particles of 1016 to 1023 and cannot distinguish the inhomogeneous reaction among individual particles (Note S1). Compared with conventional sensors, the NV-based quantum sensor is small enough (10 nm to about 1 μm) to match the size of active material particles and has the advantages of high sensitivity, wide working ranges, and inherent chemical inertness to the electrochemical environment. Therefore, it enables the detection of nanoscale electrochemical evolution in a battery. More importantly, the diamond particles can be embedded in the electrode widely to achieve multi-threaded detection and mapping of physical quantities in a large area of interest. With these unique features, NV-based quantum sensing provides a powerful tool for diagnosing battery failure and monitoring battery health at the electrode/battery level.

An *operando* battery model is designed to enable the coordination of the diamond quantum sensing system with the battery, as shown in Figure 1B (see the corresponding photo in Figure S3). A quartz cell enables the propagation of the laser, and three channels are integrated into the cell, including a working electrode, a counter electrode, and a coaxial cable for transmitting microwave pulses. During battery operation, the active material electrode undergoes Li-ion intercalation and de-intercalation associated with the variations in stress, magnetic fields, and temperature caused by changes in the volume of the electrode, the valence state of elements for the balance charge, and the generation of Joule heat. Diamond particles with ensemble NV centers are embedded in the electrode. The energy levels of the NV quantum sensor are sensitive to changes of physical quantities mentioned above (stress F, magnetic fields B, and temperature T). The changes in the NV energy levels can be detected using the well-developed technique of optically detected magnetic resonance (ODMR).[43] Subsequently, the local changes in magnetic field, temperature, and pressure can be tracked (a detailed design of the sensing scheme can be found in Note S2). In our work, we have chosen the magnetic field as the object of study, whose change can cause Zeeman splitting in the electron spin states ($m_s = \pm 1$) of the NV centers. Temperature variations cause overall shifts in the ODMR spectra, which allows us to calculate the extent of temperature changes based on the degree of the shift of ODMR spectra.

The magnetic field is chosen as the sensing target in our study, arising from the close relationship between the changes in the magnetic properties of active materials and the phase transitions induced by electrochemical reactions, which provide insights into electrochemical mechanisms.[44,45] In addition, the capacity and rate performance of $LiFePO_4$, one of the most important positive electrode materials in commercial Li-ion batteries, are strongly influenced by magnetic impurities,[46–51] especially Fe_3O_4.[52] The magnetic detection achieved through diamond NV centers promises to precisely localize and quantitatively analyze magnetic impurities within the battery electrodes and thus support the development of commercial Li-ion batteries.

Please cite this article in press as: Liu et al., *Operando* quantum sensing captures the nanoscale electrochemical evolution in batteries, Device (2024), https://doi.org/10.1016/j.device.2024.100521

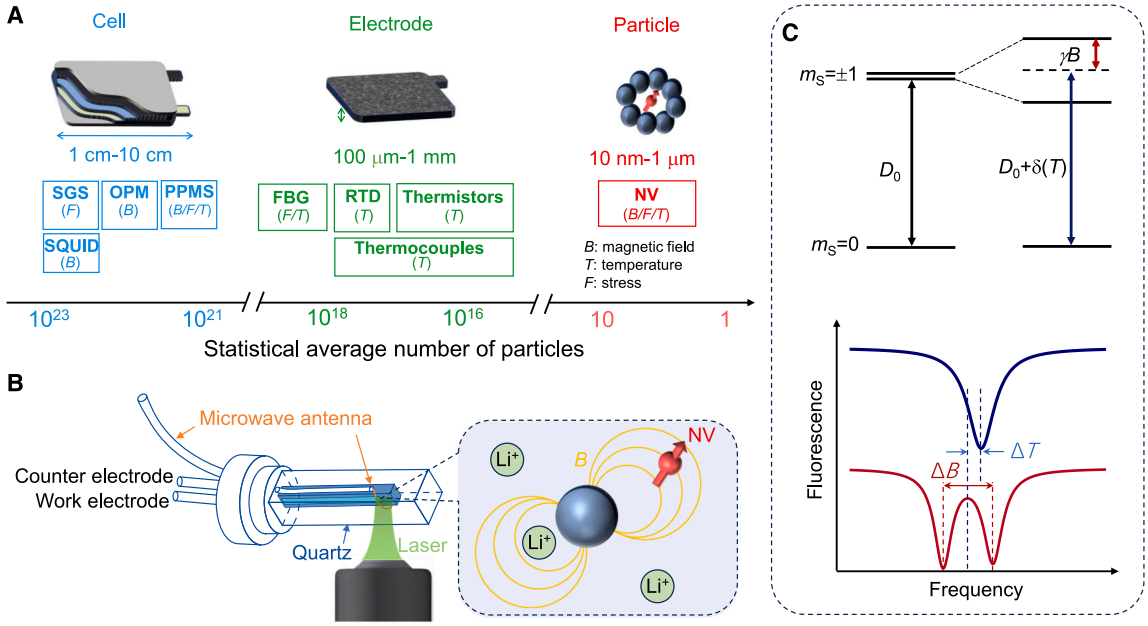

Figure 1. Schematic of the *operando* quantum sensing for the battery

(A) Comparison of different sensing techniques for battery characterization. Sensing technologies are classified according to the size of the detected area (in the number of averaged particles contributing to the sensing data) and the measurable physical quantities. SGS, strain gauge sensor; OPM, optically pumped magnetometers; SQUIDs, superconducting quantum interference devices; PPMS, physical property measurement system; FBG, fiber Bragg grating sensors; RTD, resistance temperature detector; Thermistors, thermally sensitive resistors.

(B) The device and working principle of NV-based quantum sensing. Diamond particles containing ensemble nitrogen-vacancy (NV) centers are embedded in the electrode and serve as *in situ* quantum sensors. The spin state of an NV center is sensitive to its local environment and can be optically polarized and read out through the transparent quartz window. This enables the remote detection of magnetic field, temperature, pressure, and other physical quantities within a working battery.

(C) The upper slice shows the energy levels of the ground states of an NV center. The bottom slice shows the effects of magnetic field and temperature on the ODMR spectra. A magnetic field causes a splitting between the $|m_S = \pm 1\rangle$ states, and a local change in temperature shifts the $|m_S = \pm 1\rangle$ states together.

Tracking *operando* nanoscale electrochemical evolution

To illustrate the feasibility of our scheme, we have chosen a ferromagnetic Fe_3O_4 electrode as the detection object. This choice arises from the significant toxicity to the performance of $LiFePO_4$, so exploring and analyzing its magnetism can enlighten the future use of NV sensors in solving problems with commercial Li-ion batteries. Furthermore, the multistep phase transition of Fe_3O_4 during discharge is accompanied by various magnetic transformations and the elemental valence state. It provides a representative electrochemical evolution that can be directly detected with diamond NV centers, thereby facilitating the evaluation of the application effectiveness of NV sensors inside the electrode. As shown in Figure 2A, the macroscopic characterization *in situ* X-ray diffraction (XRD) shows that the reduction of Fe_3O_4 undergoes the following three steps (1) $Fe_3O_4 + Li^+ + e^- \rightarrow FeO + Li_2O$ (the corresponding theoretical capacity is 231.5 mAh/g), (2) $FeO + e^- + Li^+ \rightarrow Fe + Li_2O$ (the corresponding theoretical capacity is 694.5 mAh/g), and (3) additional capacity due to the surface capacity of Fe/Li_2O.[8] It should be noted that the *in situ* XRD is the statistical result of many active material particles, and the inhomogeneous reaction kinetics of individual particles have been averaged out. At the same time, NV centers with much higher spatial resolution can address the abovementioned issues.

ODMR spectra are obtained by recording the fluorescence of NV centers as a function of the applied microwave frequency. To optimize the experimental parameters, we first measured zero-field ODMR spectra at different laser powers, using the zero-field splitting (D) of NV centers as a local temperature indicator. At some locations, the focused laser beam leads to an unwanted heating effect, possibly due to the carbon networks' absorption of the laser energy. To avoid the influence of the heating effect on microscale electrochemical processes, we chose a low laser power (270 μW) and kept the laser power stable during the following ODMR measurements. The microwave pulses have an imperceptible heating effect on the electrode (see Note S5 for details).

We then use diamond quantum sensors to monitor the local electrochemical reaction of a Fe_3O_4 electrode at the nanoscale. Figure 2B shows the confocal image of the electrode after diamond particles (with a diameter of about 1 μm and NV concentration of 3.5 ppm) have been embedded in the electrode. The diamond sensor P0 was marked out for further ODMR data acquirement. The measurement was started simultaneously with the discharge process of the Fe_3O_4-Li cell. A constant external magnetic field (about 89 G) was applied to enhance the magnetic signal variations resulting from the differences in the magnetic properties of the reaction products (Fe_3O_4, FeO, and Fe nanoparticles).

Please cite this article in press as: Liu et al., *Operando* quantum sensing captures the nanoscale electrochemical evolution in batteries, Device (2024), https://doi.org/10.1016/j.device.2024.100521

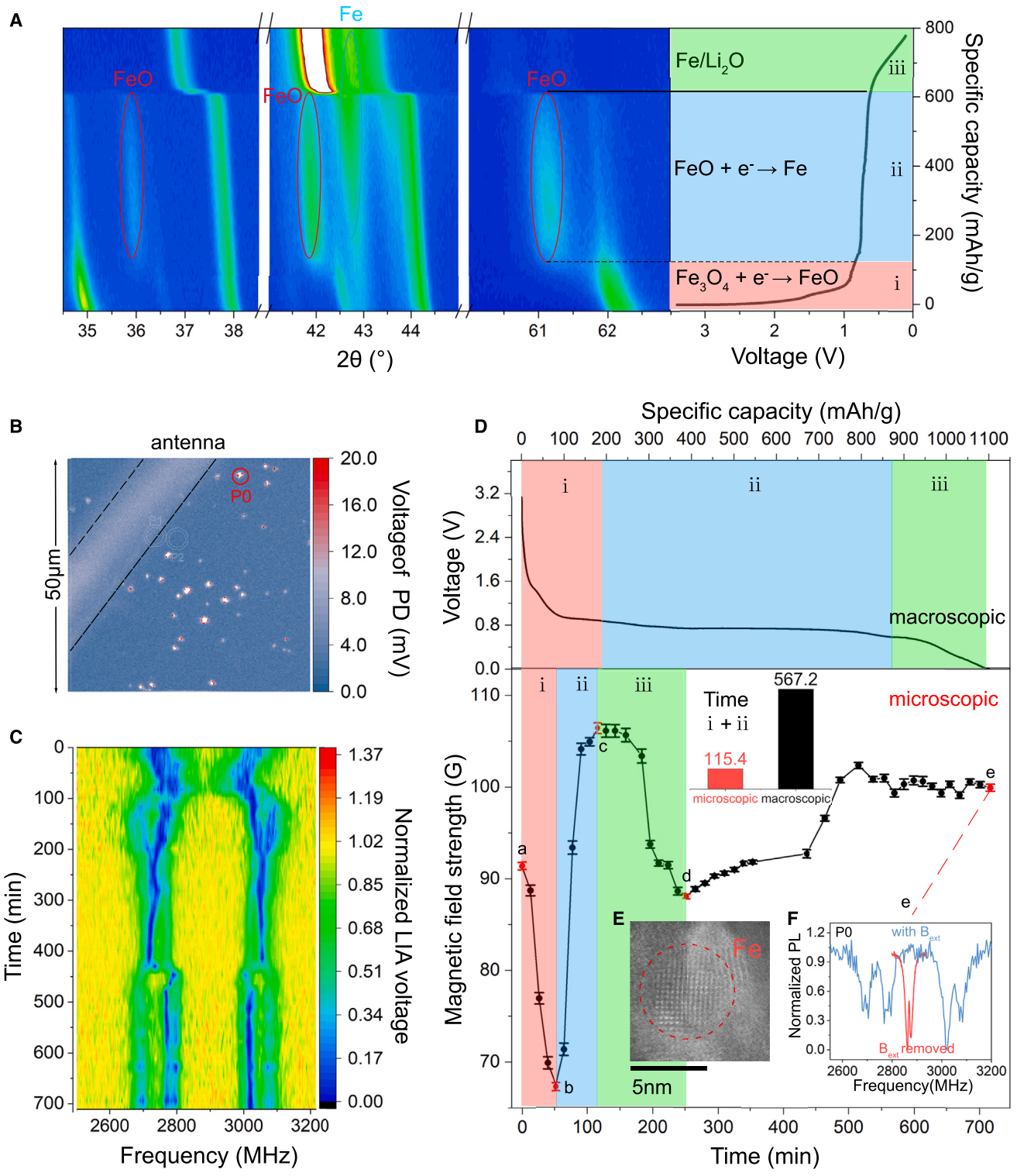

Figure 2. Diamond quantum sensors capture the nanoscale electrochemical evolution of the Fe_3O_4 electrode

(A) *In situ* XRD pattern of the Fe_3O_4 electrode.

(B) Confocal image of the electrode. Bright spots are diamond particles embedded in the electrode, of which P0 was selected for ODMR measurements. PD, photodetector.

(C) ODMR spectra were measured at P0 during battery discharge. An external magnetic field of about 88.9 G was applied. LIA, lock-in amplifier.

(legend continued on next page)

Please cite this article in press as: Liu et al., *Operando* quantum sensing captures the nanoscale electrochemical evolution in batteries, Device (2024), https://doi.org/10.1016/j.device.2024.100521

As shown in Figure 2C, ODMR spectra obtained during battery discharge show a wealth of detail and the evolution of the local magnetic field at the P0 position. The magnetic field changes sensed by the diamond NV centers mainly come from the magnetic changes of the nearest neighboring active particles rather than the overall magnetic field intensity changes because the magnetic field decays cubically in space. The ODMR spectra exhibit multiple peaks as each diamond particle contains four orientations of NV centers, with each orientation contributing a pair of resonant dips. The strength of the local magnetic field can be estimated by fitting the resonant dips of the spectra (see the details in the supplemental information).

In the first 50 min, the splitting of the resonant dips decreased rapidly, indicating a decrease in the local magnetic field (from 91.4 to 71.4 G). This is consistent with the electrochemical reaction $Fe_3O_4 + Li^+ + e^- \rightarrow Li_2O + FeO$, as the reaction products, the FeO nanoparticles, are expected to be in a paramagnetic state and have more minor magnetic susceptibility than the original Fe_3O_4 nanoparticles. In the following 65 min, the ODMR splitting recovered, and more resonant dips were observed. This stage corresponds to the reaction $FeO + Li^+ + e^- \rightarrow Fe + Li_2O$ because ferromagnetic Fe particles are magnetized (unlike paramagnetic FeO particles) under the applied external magnetic field, causing a continuous increase of the magnetic field. The local magnetic field reached a maximum of 106.4 G at 115 min, representing the full reduction of FeO particles to Fe near the P0 site. However, a considerable amount of FeO in other parts of the electrode remains unreduced at this time as the battery discharge curve shows in Figure 2D. At the macroscopic level, the overall electrochemical reaction ($Fe_3O_4 \rightarrow Fe$) took about 567 min, consistent with the work of Yu and Miao,[8] and signifies the achievement of the maximum magnetic field in the entire battery. The microscopic phase change from Fe_3O_4 to Fe at the P0 position occurred before the overall electrochemical reaction. It indicates that the phase change of Fe_3O_4 particles within the electrode does not occur uniformly, revealing significant differences in microscopic reaction kinetics.

During the latter discharge process, the magnetic field at P0 slowly decreased (c and d in Figure 2D), possibly due to the lithium storage mechanism at the Fe/Li_2O interface.[8] Subsequently, more and more FeO particles located away from P0 gradually turned to Fe, leading to a slowly increasing resultant magnetic field around the entire electrode, which explains the rise observed in the last section (d and e in Figure 2D). We performed further experiments to confirm the microscopic inhomogeneous reaction kinetics within the electrode and the correlation between the variation of the magnetic field and the phase transformation of Fe_3O_4 (see Note S4 for details). The electrochemical reduction pathway and mechanism of Fe_3O_4 are the same in both the micro and macro views, but there is a large gap in the reaction kinetics. A more plausible explanation could be related to the existing fabrication processes of the electrode, leading to microscale non-uniformities, such as variations in conductivity arising from microscale conductive networks.

Next, we used diamond NV centers as *in situ* probes to characterize the magnetic properties of the reaction products. After fully discharging the battery, the ODMR spectrum of the same diamond particle (P0) was measured (Figure 2F). An ODMR splitting of about 18.2 MHz was observed after removing the external magnetic field, indicating that the reaction products had little residual magnetism. Similar results were obtained at two other points, P1 and P3 (with a splitting of about 10 MHz, as shown in Figure S10). These results indicate that these Fe particles are not ferromagnetic but likely exhibit superparamagnetic behavior, generally observed in Fe nanoparticles smaller than 9 nm.[53] Transmission electron microscopy (TEM) images were taken to confirm the size of the reaction products. As shown in Figure 2E, the observed Fe particles were about 5 nm in diameter, well below the critical size of the superparamagnetic state for Fe particles. We also measured ODMR spectra of diamond particles at a separate electrode containing pristine Fe with a diameter of about 100 nm (see Figure S10). The pristine Fe electrode (100 nm) exhibited a clear residual magnetism (18.9 G), which is much higher than the residual magnetism (1.5 G) of the reduced Fe_3O_4 electrode shown above. Observing microscale superparamagnetic phenomena demonstrates the advantages of non-invasive *in situ* detection with NV-based quantum sensors. With its high spatial resolution and *in situ* detection capability, the NV sensor offers a new method for the non-destructive characterization of active material inside the electrode.

Multithreading monitoring inside an electrode

This section demonstrates the potential of multi-threaded quantum sensing of the magnetic field in the electrode. Figure 3A shows five diamond particles are selected and labeled in an area of about 200 × 200 (μm^2). The magnetic field map at all selected positions can be obtained in this extended area with a longer integration time. The initial distribution of the magnetic field (before discharge) is shown in Figure 3B. We can interrupt the reaction during battery discharge and perform ODMR measurements. The procedure made it possible to document the temporal variations in the magnetic field distribution, as shown in Figure 3C. The results show remarkable variations in the magnetic field's magnitude and trends among the particles. As shown in Figure 3B, the magnetic field strengths differ significantly between the individual positions (e.g., 121.6 G at P1 and 70.1 G at P4). The observed variations are probably influenced by the environmental conditions surrounding the NV sensors. Some NV sensors are close to the active materials, while others are close to the carbon network or binders. The detected magnetic field could be significantly more significant in the first

(D) The discharge profile of the Fe_3O_4-Li cell and the corresponding magnetic field evolution at P0 derived from the ODMR spectra. The electrochemical reaction process is divided into three stages ($Fe_3O_4 \rightarrow FeO \rightarrow Fe$), and the magnetic signals from the reaction products vary in each stage. The inset illustrates the duration required for the reduction of Fe_3O_4 to Fe.

(E) TEM image of the Fe_3O_4 electrode after fully discharging.

(F) ODMR spectra measured at P0 after fully discharging. The red line was measured as the external magnetic field was removed, showing the superparamagnetic behavior of the reduced Fe particles.

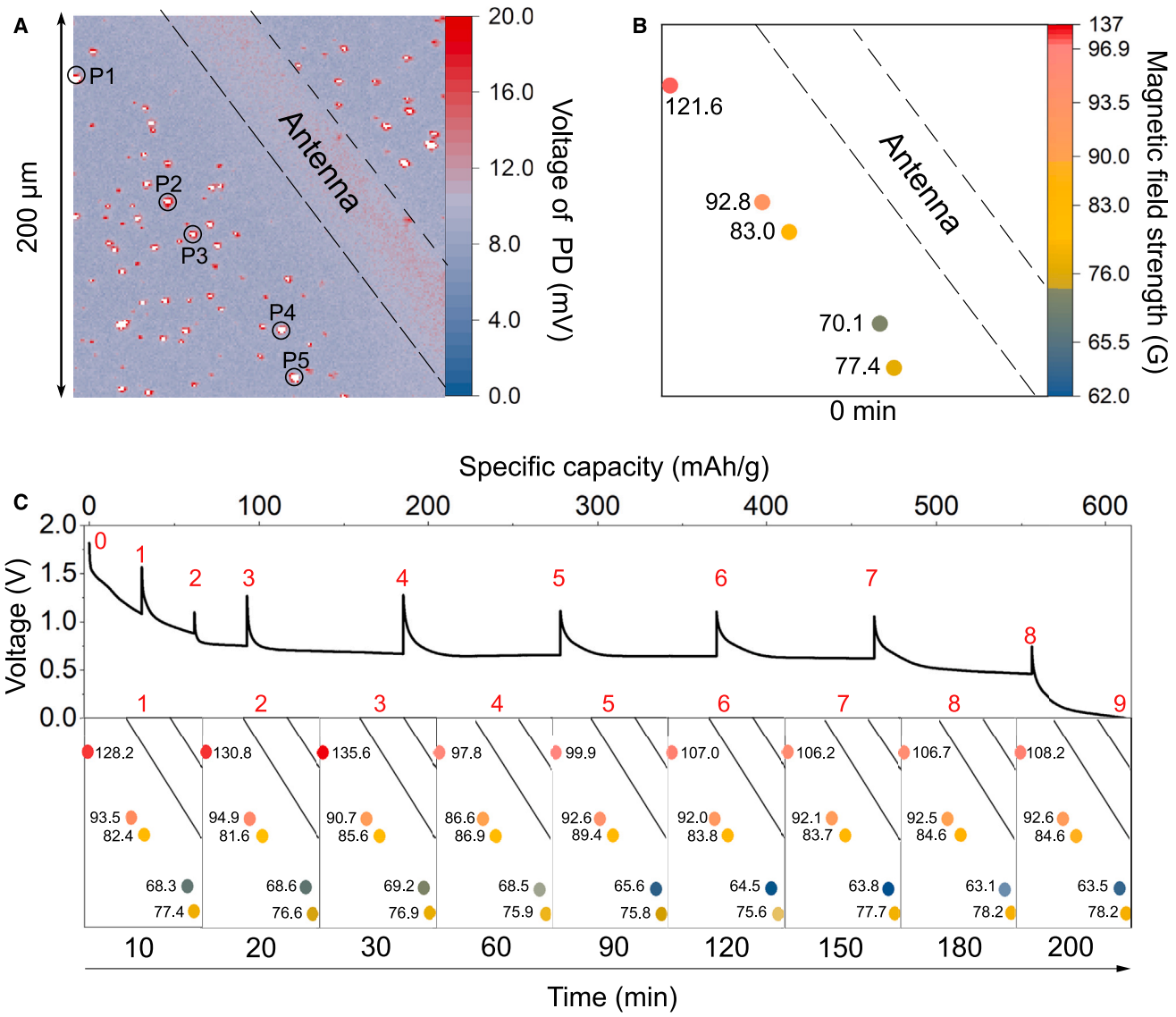

Figure 3. Magnetic field mapping inside the Fe_3O_4 electrode

(A) Confocal images of the electrode with diamond particles, of which P1–P5 are selected for the ODMR measurements.

(B) Magnetic field distribution in the Fe_3O_4 electrode at the initial moment with an external magnetic field (87.5 G).

(C) The discharge profile of the Fe_3O_4-Li cell and the corresponding variation of the magnetic field at five positions, where the numbers 0–9 represent the iterations of the magnetic field measurements.

case. It offers the possibility of using NV sensors to distinguish different electrode components. In addition, the trend of magnetic field evolution can also help to distinguish non-active materials. The magnetic field variations at P2 (maximum, 94.0 G; minimum, 90.7 G), P3 (maximum, 89.4 G; minimum, 81.6 G), P4 (maximum, 70.1 G; minimum, 63.1 G), and P5 (maximum, 78.2 G; minimum, 75.6 G) do not exceed 10%. We hypothesize that the NV sensors located at these four points are potentially affiliated with proximity to carbon networks or a binding agent instead of magnetic active material.

To summarize, the multi-threaded *in situ* detection experiments revealed significant variations in the magnetic field distribution within the battery electrodes. Using time-resolved magnetic field mapping, we can distinguish active and non-active materials based on trends in magnetic field variation. We perform diamond quantum sensing experiments with a confocal microscopy system and restrict our multi-threaded measurements to a limited number of points. In the future, we plan to advance wide-field imaging methodologies, facilitating simultaneous measurements of the entire field of view. With the further development of this technology, large-scale, high-resolution, sensitive, and real-time detection of physical parameters within the electrodes can be achieved.

DISCUSSION

In this study, we have proposed an *operando* quantum sensing method that simultaneously captures the nanoscale electrochemical evolution and monitors large regions by multi-threaded measurement. By real-time detection of the magnetic field of Fe_3O_4 particles during the electrochemical reaction, we have successfully obtained a complete picture of the phase transformation process of the electrode and observed the direct experimental evidence of the superparamagnetic state for the reduced Fe nanoparticles. Our results reveal inhomogeneous reaction kinetics within the electrode. Magnetic field mapping at multiple points within the electrode revealed the diverse nature of the active material, binder, and carbon networks within the battery structure, which would have great potential to distinguish magnetic impurities within the commercial electrode. Besides, we have preliminarily demonstrated that NV centers measure the local temperature in the battery to display the potential of our multifunctional sensing.[54] Overall, we believe that NV-based quantum sensing is promising and unique for batteries, providing detailed information from a microscopic point of view, which is crucial for promoting failure diagnosis, performance prediction, and mechanism exploration for batteries.

EXPERIMENTAL PROCEDURES

Preparation of Fe_3O_4-Li cells

All cells were assembled using 1 M $LiPF_6$ in ethylene carbonate (EC) / dimethyl carbonate (DMC) (1:1, w/w) as electrolyte without separator. To fabricate Fe_3O_4 cathode, Fe_3O_4, carbon black (CB), and polyvinylidene fluoride (PVDF) with a weight ratio of 7:1:2 in N-methyl pyrrolidinone (NMP) were mixed in an SK-300SII CE mixing machine (Shashin Kagaku) for 20 min at the speed of 2,000 rpm, producing a black slurry. The slurry was spread uniformly on a clean Cu foil and then dried. Ethanol suspension with 1-μm diamond-containing NV centers was added to the electrode by drops and the diamond accounted for 1‰ of the total electrode mass. Then the electrode was dried in air. The 100-nm Fe electrode used in Figure S10 has the same proportion of active material, CB, and PVDF and the same process. Batteries were tested at room temperature by the LAND battery test system (Wuhan, China).

Sample characterizations

In situ XRD was performed using a Bruker D8 Focus X-ray diffractometer, with measurement angle range $2\Theta = 25^\circ - 68^\circ$ and each scan cycle takes 900 s. High-resolution TEM (HRTEM) images were acquired on JEOL ARM-200F spherical aberration correction transmission electron microscope at 200 kV.

RESOURCE AVAILABILITY

Lead contact

Further information and requests for data and resources will be fulfilled by the lead contact, Prof. Liumin Suo (suoliumin@iphy.ac.cn).

Material availability

All materials used in this work are commercially available.

Data and code availability

Data are available from the corresponding author upon reasonable request.

ACKNOWLEDGMENTS

The authors thank Professor Quan Li at the Chinese University of Hong Kong for valuable discussions. This work was supported by the National Key Research and Development Program of China (2022YFB2404500 and 2019YFA0308100), the National Natural Science Foundation of China (U22B20124, 11974020, 12022509, and T2121001), the Beijing Natural Science Foundation (Z200009 and L233021), the Innovation Program for Quantum Science and Technology (2023ZD0300600), and the CAS Youth Interdisciplinary Team.

AUTHOR CONTRIBUTIONS

L.S. and G.-Q.L. supervised the project. L.S., G.-Q.L., H.Z., B.L., and X.-Q.C. conceived the idea. L.S. and B.L. designed the electrochemical experiments. G.-Q.L., H.Z., and X.-Q.C. designed the quantum sensing experiments. B.L. designed the integrated battery device for *in situ* characterization. L.S., G.-Q.L., H.Z., B.L., and X.-Q.C. improved the holistic device, including the quantum sensing system and battery device. B.L. conducted the electrochemical experiments and *in situ* XRD characterization. X.-Q.C. conducted the quantum sensing experiments. L.S., G.-Q.L., H.Z., B.L., and X.-Q.C. wrote the paper. All authors discussed the results and reviewed the manuscript.

DECLARATION OF INTERESTS

L.S., G.-Q.L., B.L., Y.-X.S., H.Z. and X.-Q.C. are co-inventors of a patent covering the design of the battery *in situ* characterization system and method based on diamond NV centers, filed by the Institute of Physics, Chinese Academy of Science.

SUPPLEMENTAL INFORMATION

Supplemental information can be found online at https://doi.org/10.1016/j.device.2024.100521.

Received: June 24, 2024
Revised: July 19, 2024
Accepted: August 5, 2024
Published: September 10, 2024

REFERENCES

1. Jangid, M.K., and Mukhopadhyay, A. (2019). Real-time monitoring of stress development during electrochemical cycling of electrode materials for Li-ion batteries: overview and perspectives. J. Mater. Chem. A Mater. *7*, 23679–23726.
2. Wei, Z., Zhao, J., He, H., Ding, G., Cui, H., and Liu, L. (2021). Future smart battery and management: Advanced sensing from external to embedded multi-dimensional measurement. J. Power Sources *489*, 229462.
3. Hendricks, C., Sood, B., and Pecht, M. (2023). Lithium-ion battery strain gauge monitoring and depth of discharge estimation. Journal of Electrochemical Energy Conversion and Storage *20*, 011008.
4. Willenberg, L.K., Dechent, P., Fuchs, G., Sauer, D.U., and Figgemeier, E. (2020). High-precision monitoring of volume change of commercial lithium-ion batteries by using strain gauges. Sustainability *12*, 557.
5. Zhu, S., Yang, L., Wen, J., Feng, X., Zhou, P., Xie, F., Zhou, J., and Wang, Y.-N. (2021). In operando measuring circumferential internal strain of 18650 Li-ion batteries by thin film strain gauge sensors. J. Power Sources *516*, 230669.
6. Wang, T., Tseng, K., Zhao, J., and Wei, Z. (2014). Thermal investigation of lithium-ion battery module with different cell arrangement structures and forced air-cooling strategies. Appl. Energy *134*, 229–238.
7. Mutyala, M.S.K., Zhao, J., Li, J., Pan, H., Yuan, C., and Li, X. (2014). In-situ temperature measurement in lithium ion battery by transferable flexible thin film thermocouples. J. Power Sources *260*, 43–49.
8. Li, Q., Li, H., Xia, Q., Hu, Z., Zhu, Y., Yan, S., Ge, C., Zhang, Q., Wang, X., Shang, X., et al. (2021). Extra storage capacity in transition metal oxide lithium-ion batteries revealed by in situ magnetometry. Nat. Mater. *20*, 76–83. https://doi.org/10.1038/s41563-020-0756-y.

9. Li, H., Hu, Z., Xia, Q., Zhang, H., Li, Z., Wang, H., Li, X., Zuo, F., Zhang, F., Wang, X., et al. (2021). Operando magnetometry probing the charge storage mechanism of CoO lithium-ion batteries. Adv. Mater. *33*, 2006629.

10. Huang, J., Blanquer, L.A., Gervillié, C., and Tarascon, J.-M. (2021). Distributed fiber optic sensing to assess in-live temperature imaging inside batteries: rayleigh and FBGs. J. Electrochem. Soc. *168*, 060520.

11. Liu, Q., Ran, Z.L., Rao, Y.J., Luo, S.C., Yang, H.Q., and Huang, Y. (2014). Highly integrated FP/FBG sensor for simultaneous measurement of high temperature and strain. IEEE Photonics Technol. Lett. *26*, 1715–1717.

12. Huang, J., Albero Blanquer, L., Bonefacino, J., Logan, E.R., Alves Dalla Corte, D., Delacourt, C., Gallant, B.M., Boles, S.T., Dahn, J.R., Tam, H.-Y., and Tarascon, J.M. (2020). Operando decoding of chemical and thermal events in commercial Na (Li)-ion cells via optical sensors. Nat. Energy *5*, 674–683.

13. Vergori, E., and Yu, Y. (2019). Monitoring of Li-ion cells with distributed fibre optic sensors. Procedia Struct. Integr. *24*, 233–239.

14. Yu, Y., Vergori, E., Worwood, D., Tripathy, Y., Guo, Y., Somá, A., Greenwood, D., and Marco, J. (2021). Distributed thermal monitoring of lithium ion batteries with optical fibre sensors. J. Energy Storage *39*, 102560.

15. Bae, C.J., Manandhar, A., Kiesel, P., and Raghavan, A. (2016). Monitoring the strain evolution of lithium-ion battery electrodes using an optical fiber Bragg grating sensor. Energ. Tech. *4*, 851–855.

16. Nascimento, M., Novais, S., Ding, M.S., Ferreira, M.S., Koch, S., Passerini, S., and Pinto, J.L. (2019). Internal strain and temperature discrimination with optical fiber hybrid sensors in Li-ion batteries. J. Power Sources *410–411*, 1–9.

17. Han, G., Yan, J., Guo, Z., Greenwood, D., Marco, J., and Yu, Y. (2021). A review on various optical fibre sensing methods for batteries. Renew. Sustain. Energy Rev. *150*, 111514.

18. Su, Y.D., Preger, Y., Burroughs, H., Sun, C., and Ohodnicki, P.R. (2021). Fiber Optic Sensing Technologies for Battery Management Systems and Energy Storage Applications. Sensors *21*, 1397. https://doi.org/10.3390/s21041397.

19. Guo, X., Guo, S., Wu, C., Li, J., Liu, C., and Chen, W. (2023). Intelligent Monitoring for Safety-Enhanced Lithium-Ion/Sodium-Ion Batteries. Adv. Energy Mater. *13*, 2203903.

20. Rondin, L., Tetienne, J.-P., Hingant, T., Roch, J.-F., Maletinsky, P., and Jacques, V. (2014). Magnetometry with nitrogen-vacancy defects in diamond. Rep. Prog. Phys. *77*, 056503.

21. Schirhagl, R., Chang, K., Loretz, M., and Degen, C.L. (2014). Nitrogen-vacancy centers in diamond: nanoscale sensors for physics and biology. Annu. Rev. Phys. Chem. *65*, 83–105.

22. Casola, F., Van Der Sar, T., and Yacoby, A. (2018). Probing condensed matter physics with magnetometry based on nitrogen-vacancy centres in diamond. Nat. Rev. Mater. *3*, 17088.

23. Barry, J.F., Schloss, J.M., Bauch, E., Turner, M.J., Hart, C.A., Pham, L.M., and Walsworth, R.L. (2020). Sensitivity optimization for NV-diamond magnetometry. Rev. Mod. Phys. *92*, 015004.

24. Liu, G.-Q., Liu, R.-B., and Li, Q. (2023). Nanothermometry with enhanced sensitivity and enlarged working range using diamond sensors. Acc. Chem. Res. *56*, 95–105.

25. Degen, C.L., Reinhard, F., and Cappellaro, P. (2017). Quantum Sensing. Reviews of modern physics *89*, 035002.

26. Fang, C.Y., Vaijayanthimala, V., Cheng, C.A., Yeh, S.H., Chang, C.F., Li, C.L., and Chang, H.C. (2011). The exocytosis of fluorescent nanodiamond and its use as a long-term cell tracker. Small *7*, 3363–3370.

27. Mohan, N., Chen, C.S., Hsieh, H.H., Wu, Y.C., and Chang, H.C. (2010). In vivo imaging and toxicity assessments of fluorescent nanodiamonds in Caenorhabditis elegans. Nano Lett. *10*, 3692–3699. https://doi.org/10.1021/nl1021909.

28. Maze, J.R., Stanwix, P.L., Hodges, J.S., Hong, S., Taylor, J.M., Cappellaro, P., Jiang, L., Dutt, M.V.G., Togan, E., Zibrov, A.S., et al. (2008). Nanoscale magnetic sensing with an individual electronic spin in diamond. Nature *455*, 644–647. https://doi.org/10.1038/nature07279.

29. Zhang, C., Shagieva, F., Widmann, M., Kübler, M., Vorobyov, V., Kapitanova, P., Nenasheva, E., Corkill, R., Rhrle, O., Nakamura, K., et al. (2021). Diamond magnetometry and gradiometry towards subpicotesla dc field measurement. Phys. Rev. Appl. *15*, 064075.

30. Le Sage, D., Arai, K., Glenn, D.R., DeVience, S.J., Pham, L.M., Rahn-Lee, L., Lukin, M.D., Yacoby, A., Komeili, A., and Walsworth, R.L. (2013). Optical magnetic imaging of living cells. Nature *496*, 486–489. https://doi.org/10.1038/nature12072.

31. Hsieh, S., Bhattacharyya, P., Zu, C., Mittiga, T., Smart, T.J., Machado, F., Kobrin, B., Höhn, T.O., Rui, N.Z., Kamrani, M., et al. (2019). Imaging stress and magnetism at high pressures using a nanoscale quantum sensor. Science *366*, 1349–1354.

32. Kucsko, G., Maurer, P.C., Yao, N.Y., Kubo, M., Noh, H.J., Lo, P.K., Park, H., and Lukin, M.D. (2013). Nanometre-scale thermometry in a living cell. Nature *500*, 54–58. https://doi.org/10.1038/nature12373.

33. Liu, G.Q., Feng, X., Wang, N., Li, Q., and Liu, R.B. (2019). Coherent quantum control of nitrogen-vacancy center spins near 1000 kelvin. Nat. Commun. *10*, 1344. https://doi.org/10.1038/s41467-019-09327-2.

34. Dou, R., Zhu, G., Leong, W.-H., Feng, X., Li, Z., Lin, C., Wang, S., and Li, Q. (2023). In operando nanothermometry by nanodiamond based temperature sensing. Carbon *203*, 534–541.

35. Toyli, D.M., de las Casas, C.F., Christle, D.J., Dobrovitski, V.V., and Awschalom, D.D. (2013). Fluorescence thermometry enhanced by the quantum coherence of single spins in diamond. Proc. Natl. Acad. Sci. USA *110*, 8417–8421. https://doi.org/10.1073/pnas.1306825110.

36. Marshall, M.C., Ebadi, R., Hart, C., Turner, M.J., Ku, M.J., Phillips, D.F., and Walsworth, R.L. (2022). High-precision mapping of diamond crystal strain using quantum interferometry. Phys. Rev. Appl. *17*, 024041.

37. Dai, J.-H., Shang, Y.-X., Yu, Y.-H., Xu, Y., Yu, H., Hong, F., Yu, X.-H., Pan, X.-Y., and Liu, G.-Q. (2022). Optically Detected Magnetic Resonance of Diamond Nitrogen-Vacancy Centers under Megabar Pressures. Chin. Phys. Lett. *39*, 117601.

38. Doherty, M.W., Struzhkin, V.V., Simpson, D.A., McGuinness, L.P., Meng, Y., Stacey, A., Karle, T.J., Hemley, R.J., Manson, N.B., Hollenberg, L.C.L., and Prawer, S. (2014). Electronic properties and metrology applications of the diamond NV- center under pressure. Phys. Rev. Lett. *112*, 047601. https://doi.org/10.1103/PhysRevLett.112.047601.

39. Dolde, F., Fedder, H., Doherty, M.W., Nöbauer, T., Rempp, F., Balasubramanian, G., Wolf, T., Reinhard, F., Hollenberg, L.C.L., Jelezko, F., and Wrachtrup, J. (2011). Electric-field sensing using single diamond spins. Nat. Phys. *7*, 459–463.

40. Cheng, Z., Ye, X., Wu, J., Yu, P., Wang, C.-J., Wang, M., Duan, C.K., Wang, Y., Shi, F., Tian, C., et al. (2023). Radio-Frequency Electric Field Sensing Based on a Single Solid-State Spin. Phys. Rev. Appl. *19*, 014057.

41. Dinani, H.T., Muñoz, E., and Maze, J.R. (2021). Sensing electrochemical signals using a nitrogen-vacancy center in diamond. Nanomaterials *11*, 358.

42. Hollendonner, M., Sharma, S., Parthasarathy, S.K., Dasari, D.B.R., Finkler, A., Kusminskiy, S.V., and Nagy, R. (2023). Quantum sensing of electric field distributions of liquid electrolytes with NV-centers in nanodiamonds. New J. Phys. *25*, 093008.

43. Gruber, A., Dräbenstedt, A., Tietz, C., Fleury, L., Wrachtrup, J., and Borczyskowski, C.v. (1997). Scanning confocal optical microscopy and magnetic resonance on single defect centers. Science *276*, 2012–2014.

44. Li, X., Zhang, L., Liu, H., Li, Q., and Hou, Y. (2023). Magnetic measurements applied to energy storage. Adv. Energy Mater. *13*, 2300927.

45. Zhao, Z., Ye, W., Zhang, F., Pan, Y., Zhuo, Z., Zou, F., Xu, X., Sang, X., Song, W., Zhao, Y., et al. (2023). Revealing the effect of LiOH on forming a SEI using a Co magnetic "probe". Chem. Sci. *14*, 12219–12230.

46. Salah, A., Mauger, A., Julien, C., and Gendron, F. (2006). Nano-sized impurity phases in relation to the mode of preparation of LiFePO4. Mater. Sci. Eng., B *129*, 232–244.

47. Denis, Y., Donoue, K., Kadohata, T., Murata, T., Matsuta, S., and Fujitani, S. (2008). Impurities in LiFePO4 and their influence on material characteristics. J. Electrochem. Soc. *155*, A526.

48. Zaghib, K., Mauger, A., Gendron, F., and Julien, C. (2008). Magnetic studies of phospho-olivine electrodes in relation with their electrochemical performance in Li-ion batteries. Solid State Ionics *179*, 16–23.

49. Shima, Y., Nakamura, T., Matsui, H., Yamada, Y., Miyauchi, H., Hashimoto, S., and Abe, K. (2010). Synthesis of LiFePO4/C Composite Particles by Gas–Solid Phase Reaction and Their Electrochemical Properties. J. Jpn. Soc. Powder Powder Metall. *57*, 729–733.

50. Xie, X., Yang, Y., Zhou, H., Li, M., and Zhu, Z. (2018). Quality monitoring methods of initial and terminal manufacture of LiFePO4 based lithium ion batteries by capillary electrophoresis. Talanta *179*, 822–827.

51. Salah, A.A., Mauger, A., Zaghib, K., Goodenough, J., Ravet, N., Gauthier, M., Gendron, F., and Julien, C.M. (2006). Reduction Fe3+ of Impurities in LiFePO4 from Pyrolysis of Organic Precursor Used for Carbon Deposition. Journal of the Electrochemical Society *153*, A1692.

52. Huang, K.-P., Fey, G.T.-K., Lin, Y.-C., Wu, P.-J., Chang, J.-K., and Kao, H.-M. (2017). Magnetic impurity effects on self-discharge capacity, cycle performance, and rate capability of LiFePO 4/C composites. J. Solid State Electrochem. *21*, 1767–1775.

53. Carvell, J., Ayieta, E., Gavrin, A., Cheng, R., Shah, V.R., and Sokol, P. (2010). Magnetic properties of iron nanoparticle. J. Appl. Phys. *107*.

54. Foy, C., Zhang, L., Trusheim, M.E., Bagnall, K.R., Walsh, M., Wang, E.N., and Englund, D.R. (2020). Wide-field magnetic field and temperature imaging using nanoscale quantum sensors. ACS Appl. Mater. Interfaces *12*, 26525–26533.